Overview of MST Reversed Field Pinch Research in Advancing Fusion Science

J.S. Sarff[1], A.F. Almagri[1], J.K. Anderson[1], V. Belykh[6], P.R. Brunsell[10], J. Boguski[1], P. Bonofiglo[1], M. Borchardt[1], D.L. Brower[2], W. Cappechi[1], B.E. Chapman[1], C. Cook[1], D. Craig[8], T. Crowley[3], J. Egedal[1], V.I. Davydenko[6], D.R. Demers[3], D.J. Den Hartog[1], A. DuBois[1], J. Duff[1], W.X. Ding[2], X. Feng[1], P. Fimognari[3], L. Frassinetti[10], R. Fridström[10], C.B. Forest[1], P. Franz[5], M. Galante[1], J.A. Goetz[1], R.W. Harvey[9], C.C. Hegna[1], S.P. Hirshman[7], D.J. Holly[1], A.A. Ivanov[6], C. Jacobson[1], J. Johnson[1], J. Kim[1], S. Kubala[1], L. Lin[2], K.J. McCollam[1], M. McGarry[1], V.V. Mirnov[1], L. Morton[1], S. Munaretto[1], T. Nishizawa[1], M.D. Nornberg[1], R. Norval[1], P.D. Nonn[1], S.P. Oliva[1], E. Parke[1], J. Polosatkin[6], M.J. Pueschel[1], J.A. Reusch[1], L.M. Reusch[1], J. Sauppe[1], O. Schmitz[1], S. Sears[1], A. Seltzman[1], C.R. Sovinec[1], D. Spong[7], H. Stephens[1], M. Tan[12], D. Theucks[1], J. Titus[4], J. Triana[1], P.W. Terry[1], G.C. Whelan[1], Z. Williams[1] and A. Xing[1]

[1]University of Wisconsin, Madison, Wisconsin, and the Center for Magnetic Self-Organization in Laboratory and Astrophysical Plasmas
[2]The University of California at Los Angeles, Los Angeles, California
[3]Xantho Technologies, LLC, Madison, Wisconsin
[4]Florida A&M University, Tallahassee, Florida
[5]Consorzio RFX, Associazione EURATOM-ENEA sulla Fusione, Padova, Italy
[6]Budker Institute of Nuclear Physics, Novosibirsk, Russia
[7]The Oak Ridge National Laboratory, Oak Ridge, Tennessee
[8]Wheaton College, Wheaton, Illinois
[9]CompX, Del Mar, California
[10]KTH Royal Institute of Technology, Stockholm, Sweden
[11]Pierce College Fort Steilacoom, Lakewood, Washington
[12]University of Science and Technology, Hefei, China

Corresponding Author: jssarff@wisc.edu

Abstract:
The reversed field pinch (RFP) offers unique capabilities that could be essential to closing gaps to fusion power. The RFP has large plasma current and small toroidal field, with $q(r) < 1$. Two key benefits arise: (1) the possibility for ohmic heating to ignition and (2) minimization of the field strength at the magnets. The material boundary can be made invisible to an inductive electric field, and the first-wall need not accommodate power injection ports or antennas. These features could help achieve a maintainable and reliable fusion power source. This overview summarizes MST results important for the advancement of the RFP as well as for improved understanding of toroidal confinement generally. Evidence for first observations of trapped-electron mode (TEM) turbulence in the RFP is obtained. Short-wavelength density fluctuations exhibit a density-gradient threshold, and GENE modeling predicts unstable TEMs. Core-localized neutral beam injection stimulates

bursty modes with both Alfvènic and EPM scaling. One mode agrees with a new analytic theory for the magnetic-island-induced Alfvèn eigenmode (MIAE), which conspires with an EPM to affect fast ion transport. At high current the RFP transitions to the quasi-single-helicity (QSH) state. A method to control the locked phase of QSH has been developed using resonant magnetic perturbations (RMP). Runaway electrons that appear without RMP are suppressed. An improved model for simultaneous interactions of multiple tearing modes and error fields has been developed. The RFP's tearing-relaxation behavior together with well-developed theory and computation create a ripe opportunity for rigorous validation of MHD models. Integrated data analysis (IDA) complements validation by maximizing the information embedded in multiple diagnostics, which is essential for future fusion development steps having limited diagnostics. Using IDA methods, meta-diagnostics that combine charge-exchange recombination spectroscopy, x-ray tomography, and Thomson scattering yield more robust measurements of Z_{eff} and T_e, critical parameters for MHD. Nonlinear studies using an extended MHD model including drift and two-fluid physics in NIMROD show features similar to MST observations, including a tendency for the MHD and Hall emf terms to oppose each other in Ohm's law, and opposition of the Maxwell and Reynolds stresses in momentum balance.

1 Introduction

The reversed field pinch (RFP) offers unique capabilities that could be critical to closing gaps to fusion power, stemming from the greater concentration of the magnetic field within the plasma. The RFP has large plasma current and small toroidal field, with $q(r) < 1$. Two key benefits arise: (1) the possibility for ohmic heating to ignition and (2) minimization of the field strength at the magnets. The RFP's large current density makes ohmic ignition and high fusion gain possible, if energy confinement is similar to that of a same-size, same-field tokamak [1]. Further, the material boundary can be made invisible to a low frequency inductive electric field, and the first-wall need not accommodate power injection ports or rf antennas. A practical energy system must be maintainable and reliable to assure high availability of power production, and ohmic heating and simpler magnets could help achieve these requirements by reducing system complexity and eliminating auxiliary heating requirements.

This overview of results from the MST program summarizes physics important for the advancement of the RFP as well as for improved understanding of toroidal magnetic confinement in general. With increasing emphasis on predictive fusion science, multi-configuration research allows the development of robust plasma models that inform inevitable physics and technological tradeoffs. It also provides a basis for continuing innovation. Topics included are the emergence of microturbulence in the RFP, energetic particle effects with neutral beam injection, integrated data analysis in support of model validation, control of helical plasma states using resonant magnetic perturbations, and magnetic self-organization physics.

2 Microturbulence in the RFP

Strong evidence for the first observations of trapped-electron mode (TEM) turbulence in the RFP is obtained through measurements of short-wavelength density fluctuations and gyrokinetic modeling [2]. Improved-confinement plasma conditions are obtained in MST using inductive profile control to minimize tearing modes that cause widespread magnetic stochasticity

[3]. When applied, inductive control decreases the magnetic fluctuation up to five-fold, and the global energy confinement time increases up to ten-fold. The achieved confinement is comparable to that expected for a tokamak plasma of the same size, field strength, and heating power [4]. The gradients in the density and temperature are increased as well. There is a strong likelihood that transport in the RFP will be ultimately limited by microturbulence once global tearing is sufficiently reduced. The observation of internal electron transport barriers associated with quasi-single-single conditions has also prompted consideration of microturbulence in the RFP [5, 6].

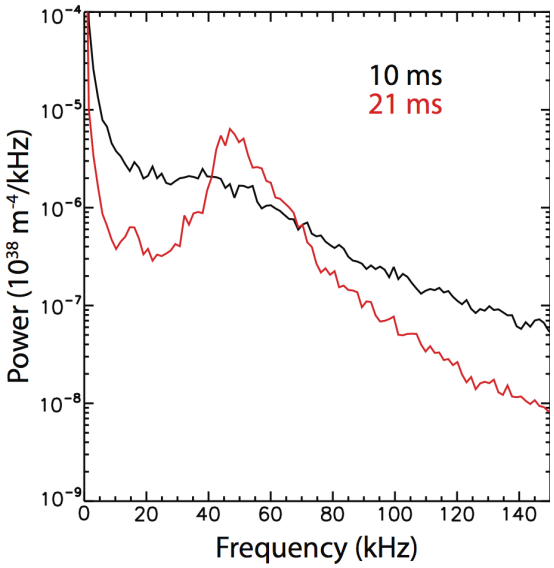

FIG. 1: Density fluctuation power spectra obtained with FIR interferometry. The data are the line-integrated fluctuations at $r/a \approx 0.85$ in standard RFP conditions before inductive control is applied (10 ms) and at the time of maximum plasma pressure during inductive control (24 ms). The density gradient is maximum at this chord location.

A new feature in density fluctuations emerges in improved-confinement MST plasmas near 50 kHz with $k_\perp \rho_i \leqslant 0.14$. The density fluctuation power spectrum for standard and improved-confinement conditions are shown in Fig. 1. The fluctuations with $f \sim 50$ kHz propagate in the electron diamagnetic drift direction and exhibit a density-gradient threshold at $R/L_n \approx 15$, as shown in Fig. 2.

Gyrokinetic modeling using the GENE code predicts unstable density-gradient-driven TEMs for these plasmas [7, 8]. The critical gradient for linear instability is close to the measured value in Fig. 2. This value is larger than for tokamak plasmas by $\sim R/a$. Nonlinear analysis with GENE predicts very strong zonal flows, and the Dimits-like up-shift for the critical gradient can be as large as $R/L_n \approx 80$. The predicted transport with large zonal flows is very small, much smaller than the observed transport level in improved-confinement MST plasmas. Since tearing modes are reduced but not completely eliminated, the impact of small magnetic perturbations has been assessed in the GENE simulations by including a small (non-stochastic) magnetic perturbation in the simulation flux-tube volume. The zonal flows are adversely affected by the radial motion induced by the magnetic perturbation, and the transport level in the nonlinearly

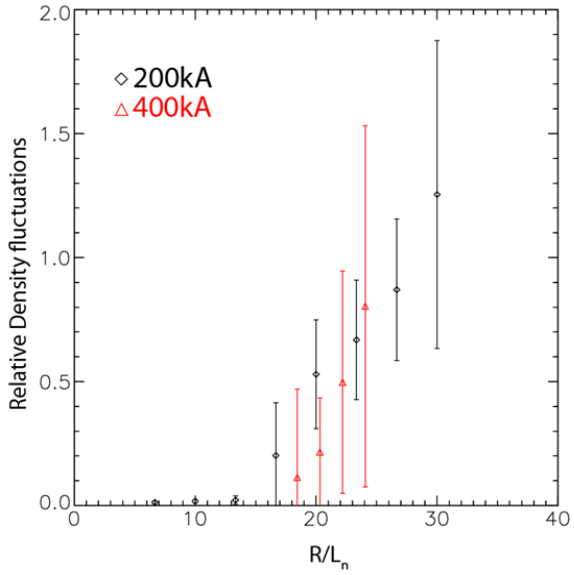

FIG. 2: Density fluctuation amplitude versus the normalized density gradient scale length, $L_n = n_e/|\nabla n_e|$. The fluctuation amplitude is for the region of maximum ∇n_e near $r/a = 0.85$. Data for low (200 kA) and moderate (400 kA) current improved-confinement plasmas are shown.

saturated turbulence increases to a value comparable to that of the experiment. The Dimits-like shift is also greatly reduced, and the nonlinear critical gradient is about 20% larger than for linear growth rates.

The observed fluctuations and their correspondence to gyrokinetic simulation predictions is strong evidence for TEM behavior in inductively controlled MST plasmas. The prediction for strong zonal flows implies that the confinement-limiting turbulence in the RFP could be much weaker in the RFP than for tokamak or stellarator plasmas, if magnetic fluctuations associated with tearing can be further suppressed. This bolsters the case for achieving tokamak-like confinement in the RFP and the possibility for ohmic heating to ignition. The zonal flow response to a magnetic perturbation suggests the application of resonant magnetic perturbations in tokamak plasmas could affect turbulent transport in similar fashion.

3 Energetic Particle Physics

MST is equipped with a 1 MW, 25 keV tangential neutral beam injection (NBI) system that creates a significant population of high $V_{||}$ fast ions localized in the core region of the plasma [9]. Previous work has shown that the fast ion confinement is very good, much larger than the thermal ion confinement due to drift effects [10]. This allows build up of a large fast ion density, and several energetic-particle-driven modes are excited that have both Alfvènic and EPM scaling characteristics [11, 12]. The features of an $m = 1$, $n = 4$ bursty mode that has Alfvènic scaling are consistent with a new analytic formulation [13] of the theory for a magnetic-island-induced Alfvèn eigenmode (MIAE) [14] associated with a gap in the Alfvèn continuum caused by magnetic island structure. An $m = 1$, $n = 5$ tearing mode is resonant

near the core in "non-reversed" MST plasmas with edge safety factor, $q(a) = 0$.

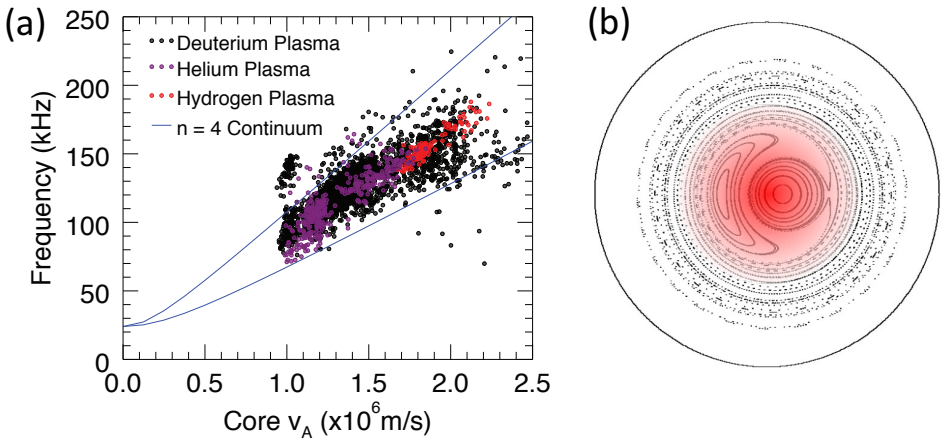

FIG. 3: (a) Measured $n = 4$ bursty mode frequency for varying NBI energy and majority ion species lies between the $j = 1$ and $j = 2$ branches of the MIAE. (b) A semi-quantitative cartoon of a poloidal cross-section illustrating the concentration of NBI-generated fast ions (red shading) in the core of an MST plasma that has a large $m = 1$ magnetic island.

The frequency scaling of the $n = 4$ bursty mode with varying Alfvén speed in hydrogen, deuterium, and helium plasmas is shown in Fig. 3(a). A cartoon of the core magnetic topology and fast ion density is shown in Fig. 3(b). The new analytic theory computes the Alfvèn continuum on helical magnetic flux surfaces located within the island separatrices. At the O-point, the continuum frequency is $f = \sqrt{f_{BAE}^2 + \frac{n^2 j(j+2)}{16} q_0'^2 W^2 k_{||}^2 V_A^2}$, where n is the toroidal mode number of the magnetic island, j is an integer that indicates the branch of the mode, q_0' is the perpendicular derivative of the safety factor at the resonant surface (magnetic shear), W is the island width, V_A is the local Alfvèn velocity, and f_{BAE} is the minimum BAE frequency at the rational surface. The mode data in MST fall between the predicted $j = 1$ and $j = 2$ continuum branches, marked by the blue lines in Fig. 3(a). Multi-chord FIR interferometry shows the mode is localized to the $q = 1/5$ region, and this MIAE conspires with an EPM to affect fast ion transport through a predator-prey mechanism [12]. The local fast ion pressure is nevertheless large with local $\beta_{fi} \approx \beta_{th}$, owing to the near-classical fast-ion confinement.

4 Controlling the Quasi-Single-Helicity State

At high current the RFP often spontaneously transitions to the quasi-single-helicity (QSH) state characterized by the growth of the inner-most resonant $m = 1$ tearing mode to large amplitude while the broadband "secondary" modes are reduced [6]. The amplitude of the dominant mode can become so large that the plasma core region contains only a helical magnetic axis, somewhat analogous to stellarator equilibria. The dominant toroidal mode number is determined by the on-axis value of the safety factor, which scales with aspect ratio as $q(0) \approx \frac{2}{3}(a/R_0)$. In MST the dominant mode is typically $n = 5$ while in RFX-mod it is typically $n = 6$ or 7.

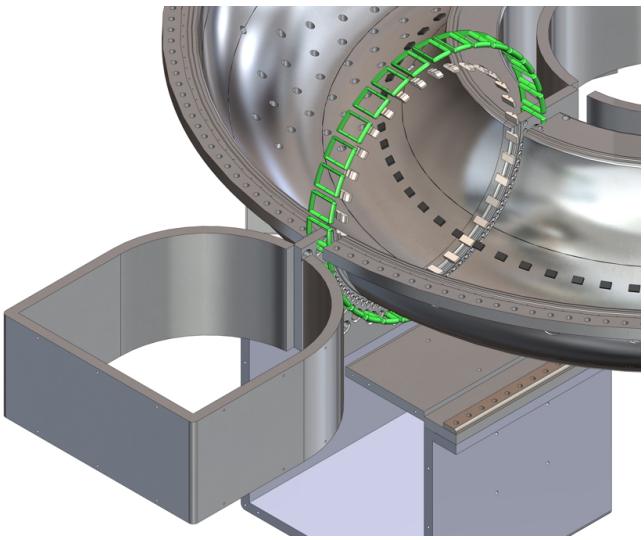

FIG. 4: SOLIDWORKS© *model of the bottom half of MST's 5-cm-thick aluminum shell in the region of the vertical cut. The error field correction coils (green) are also used to apply a toroidally localized magnetic perturbation with a precise poloidal mode,* m*. Pickup coils (pink) measure the field locally in the gap. The 64-station pickup loop array used to measure the toroidal mode spectrum is shown in black .*

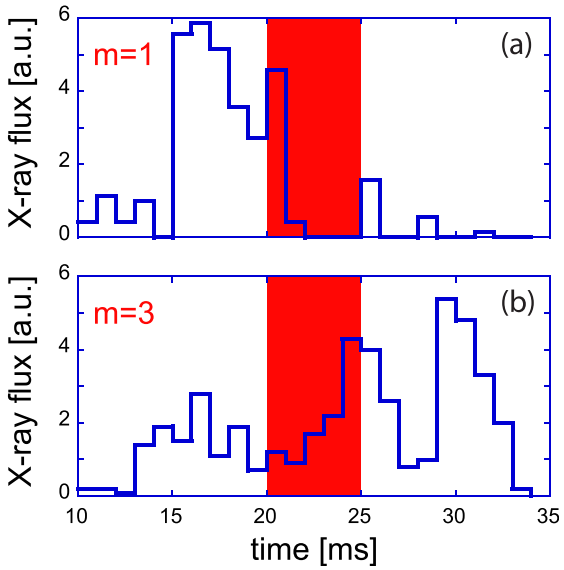

FIG. 5: Comparison of x-ray counts with (a) $m = 1$ *and (b)* $m = 3$ *magnetic perturbations. The red shaded regions correspond to the period the perturbations are applied. The implied reduction in runaway electrons is greater for resonant (*$m = 1$*) versus non-resonant (*$m = 3$*) perturbations. (see [15])*

The phase of the helical 3D structure for QSH plasmas in MST is wall-locked but varies shot-to-shot. A method has been developed to control the locked phase using $m = 1$ resonant magnetic perturbations (RMP) applied through the vertical cut in the metal shell surrounding the plasma, shown in Fig. 4 [16]. A key benefit is improved diagnosis using diagnostics that cannot simultaneously observe the 3D structure, e.g., an internal electron heat transport barrier. To apply an RMP, saddle coils that are normally used for feedback control of the local magnetic field error are programmed to produce a radial field with a given m value. Since the gap is narrow, the toroidal mode spectrum for the RMP is very broad.

An interesting property of QSH plasmas is that runaway electrons are better confined than for standard plasmas with a broad spectrum of similarly sized modes. When a resonant $m = 1$ RMP is applied of sufficient amplitude, the runaway electrons are reduced (inferred through x-ray measurements). This is interpreted as increased magnetic stochasticity in the region of the dominant mode caused by multiple RMPs. When a non-resonant $m = 3$ RMP is applied, the runaway electrons persist. This points to the importance of magnetic stochasticity in affecting the control of runaway electrons, a great concern for disruptions in tokamak plasmas [15].

An $m = 1$ RMP also affects locking of multiple tearing modes in the standard multi-helicity regime of the RFP. This is illustrated in Fig. 6. An improved model for the locking of tearing modes due to magnetic field errors has been developed that includes the interaction of multiple modes [17]. The torque balance is modeled as

$$\rho(r)\frac{\partial \Delta\Omega_\phi}{\partial t} = \frac{1}{r}\frac{\partial}{\partial r}\Big(r\mu_\perp(r)\frac{\partial \Delta\Omega_\phi}{\partial r}\Big) + \sum_n \frac{T_{EM}^{m,n}(t)}{4\pi^2 r R_0^3}\delta(r - r_s^{m,n}) \tag{1}$$

where $\Omega(r_s^{m,n}, t) = V_\phi^{m,n}/R$ is the toroidal angular velocity of tearing mode (m, n) at rational surface, $r = r_s^{m,n}$, and $T_{EM}^{m,n}$ is the torque between the tearing mode and the resonant magnetic perturbation. The single free parameter in the model is the perpendicular viscocity, $\mu_\perp(r)$, which is taken to be spatially constant. The viscosity is adjusted to give a best-fit to the measured mode velocities. The required $\mu_\perp$ as a function of the number of modes included in Eq. 1 is shown in Fig. 7.

5 Validation and Integrated Data Analysis

The RFP's tearing-relaxation behavior together with well-developed theory and computation create a ripe opportunity for the rigorous validation of MHD models [18]. Integrated data analysis (IDA) complements validation by maximizing the information embedded in multiple diagnostics, which is essential for future fusion development steps having more limited diagnostics. A crucial MHD parameter is the Lundquist number, $S = \tau_R/\tau_A$ which depends on the plasma's resistivity, $\eta \sim Z_{eff}T_e^{-3/2}$. Using IDA methods, meta-diagnostics that combine MST's charge-exchange recombination spectroscopy, x-ray tomography, and Thomson scattering yield more robust measurements of Z_{eff} and T_e. IDA is implemented for MST diagnostics using a Bayesian probability framework, which enables a combination of information from complementary diagnostics in a rigorous approach and production of the most probable estimate of a physical quantities. For example, standard single-instrument techniques to measure

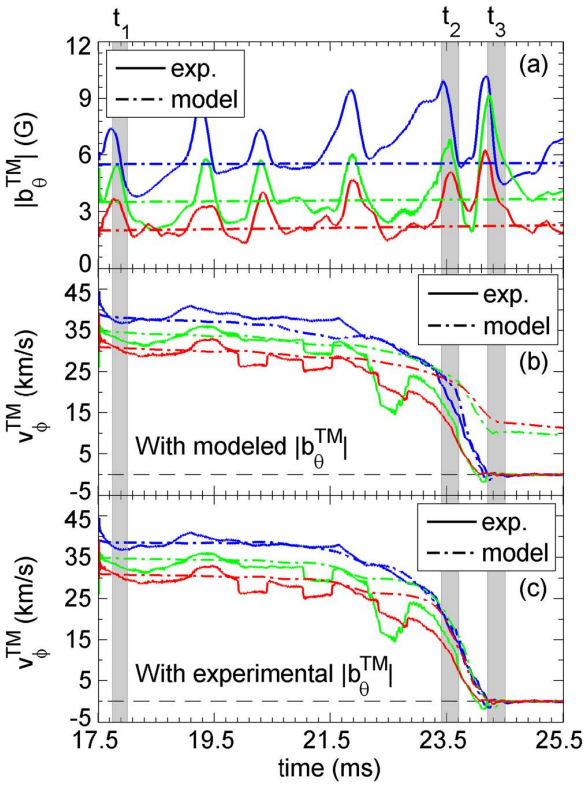

FIG. 6: Experimental and modeled tearing mode data for modes $m = 1$, $n = 6, 7, 8$ in blue, green, and red color, respectively. The (a) amplitudes of each mode and (b,c) their mode velocities. Model predictions are shown as dashed lines. In (b), the mode velocities are compared with model predictions using the modeled amplitudes in (a), while in (c) they are compared using the measured mode amplitudes in (a). The model includes the braking torques associated with eight modes, $m = 1$, $n = 6 - 13$. (see [17])

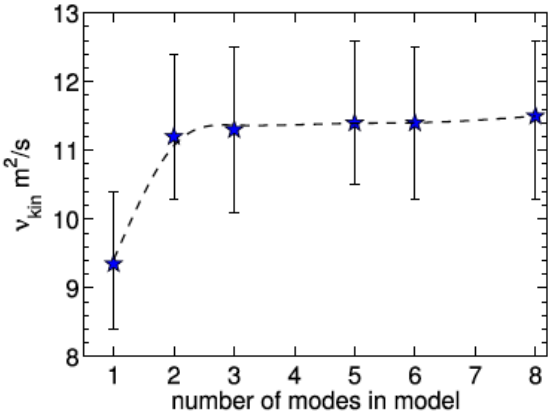

FIG. 7: Model-required kinematic viscosity for a best fit to the experimental locking time (when $V_\phi^{TM} \to 0$) versus the number of modes included in the model. The lower/upper values of error bars correspond to the best fit viscosity when the modeled plasma density is varied within its measurement uncertainty, $n_{e0} = (0.85 \pm 0.05) \times 10^{19}$ m^{-3}. (see [17])

Z_{eff} on MST all failed to provide robust and reliable measurement. However, data from different diagnostics contain some information about Z_{eff}, e.g., soft-x-ray (SXR) tomography, visible and x-ray spectroscopy, Thomson scattering background, neutral beam attenuation, direct charge-exchange recombination spectroscopy (CHERS) measurements of impurity densities, and others. IDA techniques have recently been applied on MST to combine information from CHERS and SXR to produce an improved estimate of Z_{eff} in improved-confinement plasmas [19], which is shown in Fig. 8.

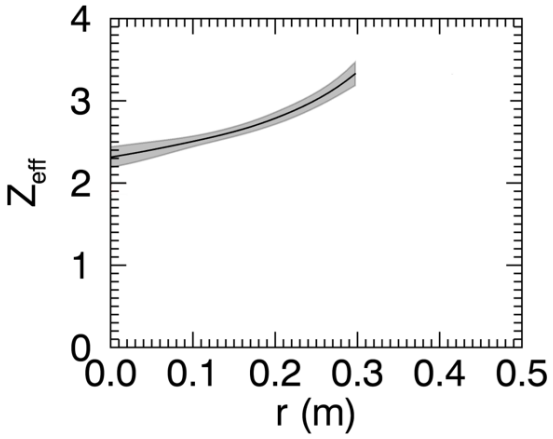

FIG. 8: Most probable radial profile of Z_{eff} in the core of MST, produced by combining data from CHERS and SXR tomography using the techniques of IDA. The gray band indicates the one-sigma uncertainty. (see [19])

6 Two-fluid Physics in Magnetic Self-Organization

The model for tearing-relaxation has recently been extended to include ion drift and two-fluid physics. This was motivated in large part by MST observations of simultaneous current and plasma flow relaxation during magnetic reconnection, and probe measurements of a large fluctuation-induced Hall dynamo emf, $\langle \widetilde{\mathbf{J}} \times \widetilde{\mathbf{B}} \rangle_{||} / en_e$, which is also proportional to the Maxwell stress for parallel ion flow.

Nonlinear computational studies using NIMROD show features similar to MST observations, including a tendency for the MHD and Hall emf terms to oppose each other in Ohm's law, and opposition of the Maxwell and Reynolds stresses in momentum balance [20]. Gyroviscosity is especially important in the RFP since the drifts are nearly completely in-surface. The dynamical behavior of the MHD and Hall e.m.f. quantities calculated in NIMROD are shown in Fig. 9 for a case with a two-fluid Ohm's law and ion gyroviscosity in momentum balance. The Lundquist number used in the simulation is somewhat lower than for typical MST plasmas. The viscosity measured in MST by methods described above is anomalous in MST, and the most appropriate value for the simulations is not well established. The NIMROD simulations produce relaxation events which are similar in character to the sawtooth process in MST plasmas. These events occur between the vertical dashed lines in Fig. 9. Note the tendency for

the opposition of the MHD and Hall dynamo e.m.f.'s in the core region for the relaxation events at $t/\tau \sim 8500$ and 10500. A specially armored "deep-insertion" probe is presently being used to measure the Hall e.m.f. over the outer half of the MST plasma. These measurements reveal a very large e.m.f. and further confirm the importance of extended MHD physics for tearing relaxation dynamics and the dynamo mechanism in the RFP.

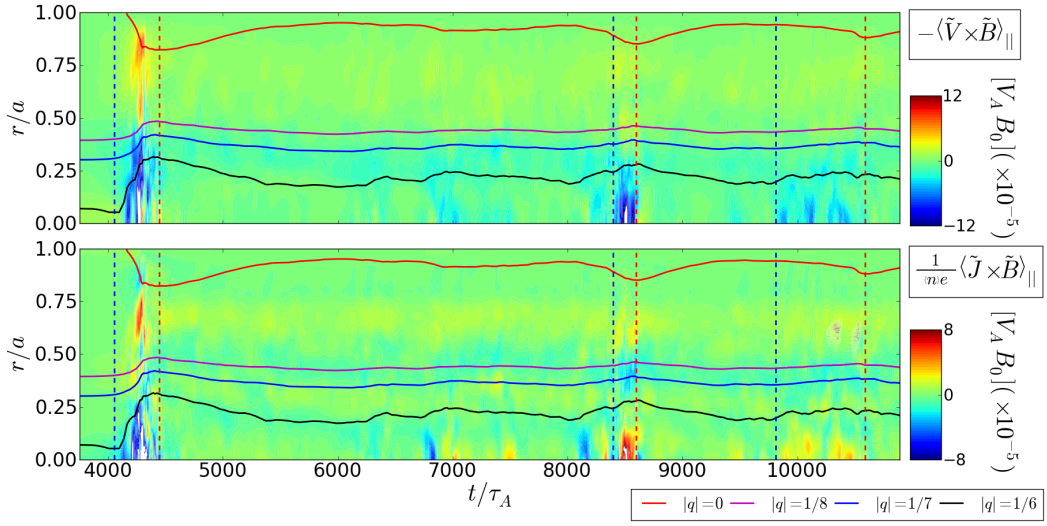

FIG. 9: Time evolution of the profiles for the MHD dynamo e.m.f., $\langle\widetilde{\mathbf{V}}\times\widetilde{\mathbf{B}}\rangle_{||}$, and the Hall dynamo e.m.f., $\langle\widetilde{\mathbf{J}}\times\widetilde{\mathbf{B}}\rangle_{||}/en_e$, for extended MHD simulations using NIMROD. The Lundquist number is $S = 20,000$, the magnetic Prandtl number is $P_m = 1$, and the normalized ion skin depth is $d_i/a = 0.17$. Ion gyroviscocity is also included. Relaxation events are bounded by the dotted lines, and the radial location of resonant surfaces for dominant tearing modes are identified by colored lines (see [20]).

7 Acknowledgements

The work reported here was supported by the U.S. DoE under Awards DE-FC02-05ER54814 DE-FG02-85ER53212, DE-FG02-01ER54615, and by the NSF under Award Number PHY-0821899. Portions were accomplished with the use of infrastructure of Complex DOL (BINP, Russia).

References

[1] J. P. Christiansen and K. V. Roberts, "Power balance in an Ohmically heated fusion reactor," Nucl. Fusion **22**, 77 (1982), 00004.

[2] D.L. Brower, "Evidence for Trapped Electron Mode Turbulence in MST Improved Confinement RFP Plasmas Evidence for Trapped Electron Mode Turbulence in MST Improved Confinement RFP Plasmas," EXC/P5, this conference, 2016.

[3] J. S. Sarff, A. F. Almagri, J. K. Anderson, T. M. Biewer, A. P. Blair, M. Cengher, B. E. Chapman, P. K. Chattopadhyay, D. Craig, D. J. DenHartog, F. Ebrahimi, G. Fiksel, C. B. Forest, J. A. Goetz, D. Holly, B. Hudson, T. W. Lovell, K. J. McCollam, P. D. Nonn, R. O'Connell, S. P. Oliva, S. C. Prager, J. C. Reardon, M. A. Thomas, M. D. Wyman, D. L. Brower, W. X. Ding, S. D. Terry, M. D. Carter, V. I. Davydenko, A. A. Ivanov, R. W. Harvey, R. I. Pinsker, and C. Xiao, "Tokamak-like confinement at a high beta and low toroidal field in the MST reversed field pinch," Nucl. Fusion **43**, 1684 (2003).

[4] B. Chapman, J. Ahn, A. Almagri, J. Anderson, F. Bonomo, D. Brower, D. Burke, K. Caspary, D. Clayton, S. Combs, W. Cox, D. Craig, B. Deng, D. Den Hartog, W. Ding, F. Ebrahimi, D. Ennis, G. Fiksel, C. Forest, C. Foust, P. Franz, S. Gangadhara, J. Goetz, M. Kaufman, J. Kulpin, A. Kuritsyn, R. Magee, M. Miller, V. Mirnov, P. Nonn, R. O'Connell, S. Oliva, S. Prager, J. Reusch, J. Sarff, H. Stephens, M. Wyman, and T. Yates, "Improved-confinement plasmas at high temperature and high beta in the MST RFP," Nucl. Fusion **49**, 104020 (2009).

[5] I. Predebon, F. Sattin, M. Veranda, D. Bonfiglio, and S. Cappello, "Microtearing Modes in Reversed Field Pinch Plasmas," Phys. Rev. Lett. **105**, 195001 (2010), 00037.

[6] R. Lorenzini, E. Martines, P. Piovesan, D. Terranova, P. Zanca, M. Zuin, A. Alfier, D. Bonfiglio, F. Bonomo, A. Canton, S. Cappello, L. Carraro, R. Cavazzana, D. F. Escande, A. Fassina, P. Franz, M. Gobbin, P. Innocente, L. Marrelli, R. Pasqualotto, M. E. Puiatti, M. Spolaore, M. Valisa, and N. Vianello, "Self-organized helical equilibria as a new paradigm for ohmically heated fusion plasmas," Nature Phys. **5**, 570 (2009).

[7] D. Carmody, M. J. Pueschel, J. K. Anderson, and P. W. Terry, "Microturbulence studies of pulsed poloidal current drive discharges in the reversed field pinch," Physics of Plasmas (1994-present) **22**, 012504 (2015).

[8] P. W. Terry, D. Carmody, H. Doerk, W. Guttenfelder, D. R. Hatch, C. C. Hegna, A. Ishizawa, F. Jenko, W.M. Nevins, I. Predebon, M. J. Pueschel, J. S. Sarff, and G. G. Whelan, "Overview of gyrokinetic studies of finite- microturbulence," Nucl. Fusion **55**, 104011 (2015).

[9] J.K. Anderson, "An island-induced Alfven eigenmode and effects of nonaxisymmetry on fast ions in the RFP," EXC/P5, this conference, 2016.

[10] J. K. Anderson, A. F. Almagri, V. Belykh, V. I. Davydenko, D. J. Den Hartog, S. Eilerman, C. B. Forest, G. Fiksel, A. A. Ivanov, J. J. Koliner, L. Lin, D. Liu, V. V. Mirnov, L. A. Morton, M. D. Nornberg, E. Parke, S. V. Polosatkin, J. A. Reusch, H. Sakakita, J. S. Sarff, D. A. Spong, N. Stupishin, J. Titus, Y. A. Tsidulko, and J. Waksman, "Fast ion confinement and stability of an NBI-Heated RFP," Phys. Plasmas **20**, 056102 (2013).

[11] J. J. Koliner, C. B. Forest, J. S. Sarff, J. K. Anderson, D. Liu, M. D. Nornberg, J. Waksman, L. Lin, D. L. Brower, W. X. Ding, and D. A. Spong, "Fast Particle Driven Alfvenic Modes in a Reversed Field Pinch," Phys. Rev. Lett. **109**, 115003 (2012).

[12] L. Lin, J. K. Anderson, D. L. Brower, W. Capecchi, W. X. Ding, S. Eilerman, C. B. Forest, J. J. Koliner, D. Liu, M. D. Nornberg, J. Reusch, and J. S. Sarff, "Energetic-particle-driven instabilities and induced fast-ion transport in a reversed field pincha)," Physics of Plasmas (1994-present) **21**, 056104 (2014).

[13] C. R. Cook and C. C. Hegna, "Analytical theory of the shear Alfvén continuum in the presence of a magnetic island," Physics of Plasmas (1994-present) **22**, 042517 (2015).

[14] A. Biancalani, L. Chen, F. Pegoraro, and F. Zonca, "Continuous Spectrum of Shear Alfvén Waves within Magnetic Islands," **105**, 095002.

[15] S. Munaretto, B. E. Chapman, M. D. Nornberg, J. Boguski, A. M. DuBois, A. F. Almagri, and J. S. Sarff, "Effect of resonant magnetic perturbations on three dimensional equilibria in the Madison Symmetric Torus reversed-field pinch," Physics of Plasmas (1994-present) **23**, 056104 (2016).

[16] S. Munaretto, B. E. Chapman, D. J. Holly, M. D. Nornberg, R. J. Norval, D. J. Den Hartog, J. A. Goetz, and K. J. McCollam, "Control of 3D equilibria with RMPs in MST," accepted for publication Plasma Phys. Control. Fusion (2015).

[17] R. Fridström, S. Munaretto, L. Frassinetti, B. E. Chapman, P. R. Brunsell, and J. S. Sarff, "Tearing mode dynamics and locking in the presence of external magnetic perturbations," Physics of Plasmas (1994-present) **23**, 062504 (2016).

[18] D. Den Hartog, "Enhanced measurements for MHD validation using integrated data analysis on the MST fusion research experiment," EXD/P5-6, this conference, 2016.

[19] M. E. Galante, L. M. Reusch, D. J. Den Hartog, P. Franz, J. R. Johnson, M. B. McGarry, M. D. Nornberg, and H. D. Stephens, "Determination of $Z_{\rm eff}$ by Integrating Measurements from X-ray tomography and Charge Exchange Recombination Spectroscopy," submitted to Nucl. Fusion (2015).

[20] J. Sauppe, *Extended MHD Modeling of Plasma Relaxation Dynamics in the Reversed-Field Pinch*, Ph.D. thesis, University of Wisconsin-Madison (2015).